# Chapter 3

# Numerical Investigation of Piled-Raft Foundation Behaviour

## 3.1 Introduction

Since the emergence of high-processing computational systems and the development of various commercial codes, numerical methods have become the most popular analysis approach. Among these methods, 3D finite element (FE) analysis has been widely recognized as a versatile tool for studying complex problems. However, its implementation requires high-processing units and expertise in utilizing the available codes, such as PLAXIS, FLAC, and ABAQUS, which have been used in recent years to investigate piled-raft foundation models, including their intricate interaction behaviour.

This chapter aims to analyze three-dimensional model of a piled-raft foundation. A series of such models were numerically examined using ABAQUS, a program originally developed by Dassault Systemes (Smith, 2009). Selecting ABAQUS over other specialized geotechnical software for piled raft foundation analysis offers versatility across engineering disciplines, comprehensive assessment of superstructure-soil interaction, seamless integration with the SIMULIA suite and CAD software, robust handling of complexity, and access to advanced analysis features crucial for accurately simulating geotechnical behaviours. It allows for the consideration of any potential super-structural effects, which could be a subject for future study. Based on finite element analysis, ABAQUS offers advanced modelling across a wide range of engineering domains, including structural analysis, contact analysis, composite analysis, fracture mechanics, and non-linear analysis.

The present numerical model was first validated through experimental analysis discussed in the literature (Vakili, 2015), considering the interaction between piles, raft, and the soil medium. Furthermore, the study investigated the influence of various parameters on settlements. These parameters included the geometrical properties of the foundation elements, such as pile length, diameter, number, raft thickness, and soil characteristics like cohesion and internal friction angle. The findings from such investigations could potentially contribute to the economical design of foundations.

The ABAQUS software was utilized to create a 3D model of a piled-raft foundation. The entire model can be categorized into three distinct parts: the soil continuum, the raft, and a group of piles. The soil supporting the foundation was modelled as a large cuboid block, while the raft and piles were attached and modelled together. Subsequently, the pile group was embedded into the soil medium. For the simulation, the soil continuum was modelled using the Mohr-Coulomb model, which is a plastic model. The Mohr-Coulomb model is chosen due to its simplicity, widespread empirical validation, and ease of parameter interpretation, making it a practical and efficient choice for simulating soil behavior in engineering applications. A concise overview of this model is provided later in this chapter.

In contrast to pile foundations, where piles primarily bear the load, piled-raft foundations distribute a portion of the total load to both the raft and the piles. Piled-raft foundations have emerged as a favourable choice in recent years, particularly for high-rise constructions. This is due to a better understanding of the load-sharing behaviour in piled rafts and their successful field applications in countries such as Germany, UAE, Japan, and others.

Furthermore, the literature highlights that, despite its time-consuming nature, 3D modeling yields better results compared to 2D modeling. Therefore, a three-dimensional analysis should be prioritized when high-performance computers with simulation capabilities are available.

## 3.2 Modules of Finite Element Modelling in ABAQUS

The typical numerical modelling process in ABAQUS adheres to the modules illustrated in Figure 3.1. These modules are briefly described in the subsequent sections (Abaqus/CAE User's Manual).

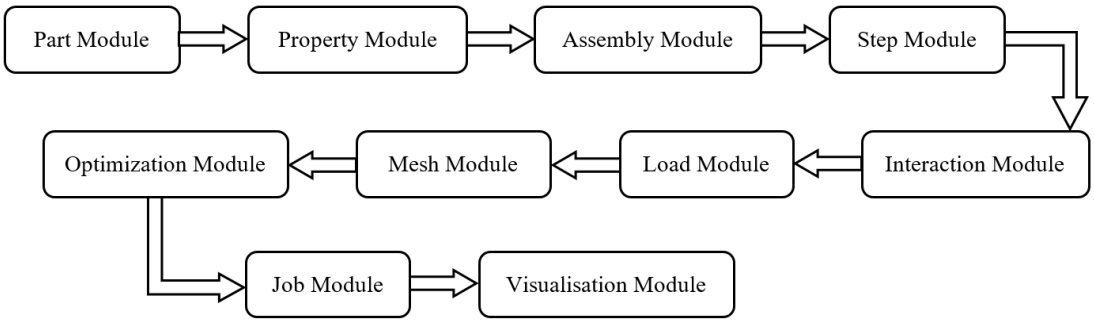


Figure 3.1: Modules in ABAQUS

### (a) Part module

The Part Module in ABAQUS serves as an interface for creating the necessary model geometries in one or multiple parts. It offers various shape features, including solids, shells, wires, cuts, and blends, to facilitate the creation of these parts. The module provides options for choosing deformable, rigid, or Eulerian parts, allowing for modification, creation, and management of the associated parts. Additionally, it enables the importation of parts from third-party formats.

### (b) Property module

The Property Module facilitates the definition of material properties for the parts. While ABAQUS does not provide pre-defined material attributes, users can create a library or use plugins. Additionally, ABAQUS offers a range of material models, including mechanical, thermal, electrical, and more, which can be employed to create desired materials. The material data is subsequently defined and assigned to the relevant model parts.

**(c) Assembly module**

The Assembly Module in ABAQUS serves the purpose of combining multiple instances of parts into a single assembly. The individual part instances are positioned relative to each other within a global coordinate system by employing specific translations, rotations, and other position constraints. Boundary conditions, stresses, and meshing are applied within this assembly.

**(d) Step module**

The analysis steps of any model are created in the Step Module. The steps begin with an initial step to define the predefined fields, boundary conditions and involved interaction. Other steps are then sequentially defined for the required loadings. This module also allows to specify output requests and analysis controls per needs.

**(e) Interaction Module**

The Interaction Module in ABAQUS plays a crucial role in defining the relationships between various elements within a model. This module offers a range of interaction types, including general contact, surface-to-surface contact, elastic foundation, tie constraints, springs, dashpots, and more. These interactions can be considered active in specific analysis steps, making them step-dependent and allowing for precise control over the simulation.

**(f) Load module**

The Load Module defines and manages loads, boundary conditions, and predefined fields. This module encompasses a variety of loads, such as concentrated loads and moments, as well as boundary conditions that can involve displacement, rotation, symmetry, antisymmetry, or encastre. Loading steps can be defined by external forces acting on the body or its components, as well as internal forces like the self-weight of the body. The Load Module provides the necessary tools to effectively specify and control these load and boundary condition parameters.

**(g) Mesh module**

The Mesh Module enables the meshing of assemblies or individual parts. It provides options for seeding, selecting meshing techniques (such as free, structured, and sweep), and choosing element types. Different meshing techniques are visually distinguished by colours in Abaqus. If desired, these techniques can be modified by partitioning a part into simpler components.

**(h) Optimization module**

The Optimization Module optimises models according to a defined set of objectives and constraints. It offers two main types of optimization: topology optimization and shape optimization. Topology optimization focuses on modifying the density and stiffness of components in the original design, resulting in a new material distribution that meets the desired objectives. On the other hand, shape optimization involves altering the geometry of the model by repositioning surface nodes and reducing stress concentration areas. These optimization techniques in ABAQUS allow for enhanced design and improved model performance.

**(i) Job module**

The Job Module in ABAQUS analyses the created model after completing overall definition tasks, including geometry, properties, and contact specifications. This module allows for the execution of multiple analyses simultaneously, and the progress of each analysis can be monitored at any given moment.

**(j) Visualisation module**

The Visualization Module serves as the final module, enabling the viewing of analysis results. It presents the results based on the defined output requests, allowing for the creation of X-Y plots to visualize the desired data. Additionally, it can showcase the model animation in a movie-like format.

## 3.3 Modelling of Piled-Raft Foundation System in ABAQUS

### 3.3.1 Geometric modelling

Figure 3.2 presents a visual representation of a piled-raft foundation situated above a soil medium. When simulating the piled-raft foundation on soil, it's possible to work with the entire model or just a portion of it due to its symmetry. The depiction features dashed lines outlining a specific quarter-section within the entire conceptual model. By capitalizing on inherent symmetry, the analytical focus narrows to this singular quadrant. This strategic reduction in analysis scope significantly enhances computational efficiency and expedites the assessment process.

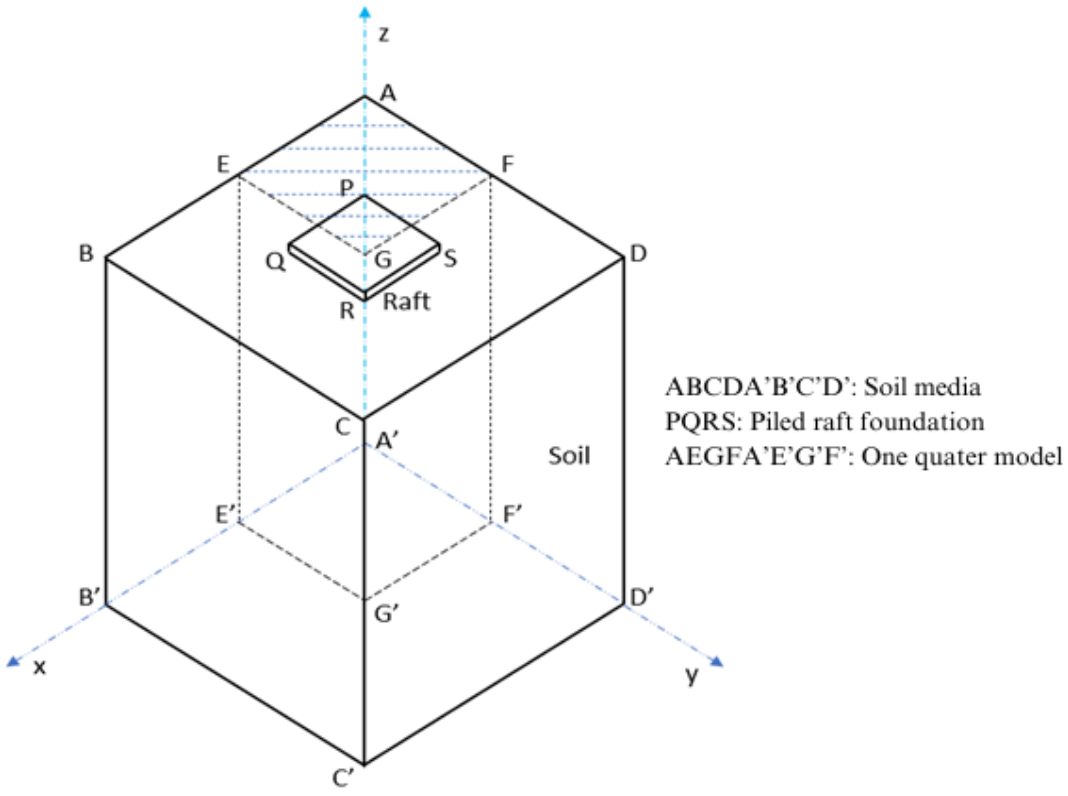


Figure 3.2: Schematic diagram of piled-raft foundation

Establishing acceptable boundary extents and conditions for the chosen continuum is crucial while developing the soil continuum model. This is necessary to enhance

the computational efficiency of the numerical simulation. Moreover, appropriate boundary conditions are essential to establish a controlled and realistic simulation environment.

In modelling piled raft foundation system, the bottom of the continuum is restrained in all-directions. The symmetry conditions along the central axis are represented by XSIMM and YSIMM, which signify symmetry along the respective planes. At the side faces, movement along the x-axis within the yz plane and movement along the y-axis within the xz plane are constrained, indicating the roller support.

### 3.3.2 Material modelling

Material modelling of soil continuum is a fundamental aspect of geotechnical engineering, enabling researchers to understand and predict the mechanical behaviour of soil under different loading conditions. As a complex material, soil displays contrasting behaviours in two primary scenarios: the elastic and plastic ranges.

In the elastic case of material modelling for soil continuum, the soil is assumed to behave linearly within the elastic limit, adhering to Hooke's law. This means that when a load is applied to the soil, it will deform proportionally and elastically in response. Elastic constants characterize the stress-strain relationship in this elastic range, Young's modulus ($E$) and Poisson's ratio ($\nu$).

Most of the earlier research employed a linear elastic constitutive model for soil applying Hooke's law, which suggests a direct proportionality between normal stress ($\sigma$) and normal strain ($\epsilon$), represented as follows:

$$\sigma = E\epsilon \tag{3.1}$$

In a $3D$ space, both stress and strain have nine components, representing normal and shear stresses/strains along three principal axes ($x, y$, and $z$). Hooke's law in

$3D$ space can be represented in matrix form as follows:

$$\begin{Bmatrix} \epsilon_{xx} \\ \epsilon_{yy} \\ \epsilon_{zz} \\ \epsilon_{xy} \\ \epsilon_{xz} \\ \epsilon_{yz} \end{Bmatrix} = \frac{1}{E} \begin{bmatrix} 1 & -\nu & -\nu & 0 & 0 & 0 \\ -\nu & 1 & -\nu & 0 & 0 & 0 \\ -\nu & -\nu & 1 & 0 & 0 & 0 \\ 0 & 0 & 0 & 1+\nu & 0 & 0 \\ 0 & 0 & 0 & 0 & 1+\nu & 0 \\ 0 & 0 & 0 & 0 & 0 & 1+\nu \end{bmatrix} \begin{Bmatrix} \sigma_{xx} \\ \sigma_{yy} \\ \sigma_{zz} \\ \sigma_{xy} \\ \sigma_{xz} \\ \sigma_{yz} \end{Bmatrix} \tag{3.2}$$

Poisson's ratio,

$$\nu = \frac{\text{lateral strain}}{\text{longitudinal strain}} = -\frac{\epsilon_{yy}}{\epsilon_{xx}} = -\frac{\epsilon_{zz}}{\epsilon_{xx}} \tag{3.3}$$

The classical elastic theory was developed for homogeneous and isotropic materials like steel, iron, and rubber, where strong ionic bonds keep them within the elastic limit. However, a three-phase, anisotropic, and non-homogenous material with limited cohesion or bonding in the case of granular soil, cannot be fully described by pure elastic theory. Hence, researchers utilize models that integrate elements of elasticity and plasticity to represent soil behaviour accurately.

Models provide a mathematical representation of material behaviour, influencing crucial aspects of their mechanical response. ABAQUS provides several plasticity models that allow users to simulate the non-linear behaviour of materials, including plastic deformation and failure. The plastic models provided by ABAQUS include the Mohr-Coulomb model, Drucker-Prager model, Cam-Clay Model, Cap Plasticity Model and several others.

The Mohr-Coulomb model is a highly suitable linear elastic-plastic representation, requiring five input parameters to characterize stress-strain behaviour. The model exhibits linear stress-strain behaviour in the elastic range, governed by two parameters derived from Hooke's law: Young's modulus ($E$) and Poisson's ratio ($\nu$). When the stress state exceeds the yield surface, plastic deformation occurs, and the soil exhibits non-linear behaviour. Friction angle ($\phi$) and cohesion ($c$) establish the

failure criteria, while dilatancy angle ($\psi$) characterises the flow rule. It stands as one of the prevailing plasticity models extensively employed in geotechnical analysis to simulate soil behaviour. This model is grounded on the fundamental principles of the Mohr-Coulomb failure criterion, which governs the shear strength of a material under varying stress conditions.

The Mohr-Coulomb failure envelope represents the shear strength of soil determined through multiple triaxial tests, identifying the plane at which failure occurs (Figure 3.3). The Mohr-Coulomb failure criterion is expressed as an equation that defines the line representing the failure envelope. The general form of the equation is:

$$\tau_f = c + \sigma_f \cdot \tan\phi \tag{3.4}$$

Here, $\tau_f$ and $\sigma_f$ represent the shear and normal stresses, respectively, acting on the failure plane. $c$ denotes the apparent cohesion, while $\phi$ indicates the angle of internal friction. $\sigma_1$ and $\sigma_3$ represent the maximum and minimum principal stresses, respectively.

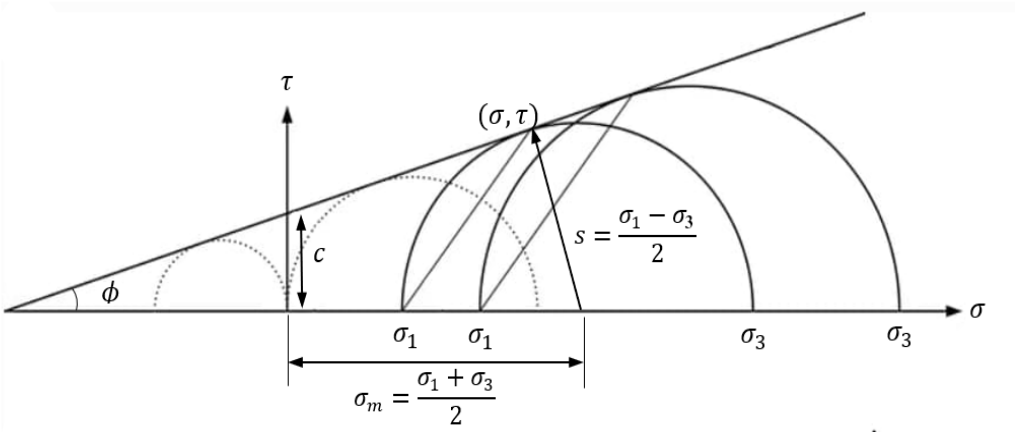


Figure 3.3: Mohr-Coulomb Model

### 3.3.3 Modelling of the interfaces

Modelling of the interfaces is a crucial aspect of simulating realistic and accurate structural interactions in FE analysis. The contact zone represents the region where

two or more bodies make contact, making it vital to precisely capture the mechanical behaviour in these regions to ensure dependable simulation outcomes. ABAQUS offers a range of contact formulations and options to represent the contact behaviour between surfaces effectively.

The analysis of piled raft foundations includes three distinct contact zones involving the interaction between soil, raft, and piles. These contact zones are known as pile-raft, raft-soil, and pile-soil interfaces. Modelling these contact surfaces requires calculating the friction factor, which relies on factors like adhesion, porosity, and surface roughness.

Among the various methodologies documented in the literature, Das (2007) discussed the empirical $\alpha, \beta$ and $\gamma$ methods specifically in the context of clay. According to the $\alpha-$ method, the friction factor $(f)$ can be computed using the equation,

$$f = \alpha c_u \tag{3.5}$$

where $\alpha$ represents an empirical coefficient, and $c_u$ corresponds to the undrained shear strength. However, in the case of sand, the computation of the friction factor is done using the following expressions:

$$\begin{aligned} f &= K\sigma'_z \tan\delta \quad \text{for} \quad z = 0 \quad \text{to} \quad L' \\ f &= f_{z=L'} \quad \text{for} \quad z = L' \quad \text{to} \quad L \end{aligned} \tag{3.6}$$

For bored piles, $K = 1 - \sin\phi$

Here, $K$ stands for the earth coefficient, $\sigma'_z$ for the effective vertical stress at depth $z$, $\delta$ for the soil-pile friction angle and $\phi$ for the angle of internal friction.$L$ denotes the overall length of the piles, whereas $L'$ corresponds to the critical depth, which can be approximately 15 to 20 times the diameter of the pile.

Issues pertaining to interfaces include the formulation of geometry, the definition of

interface laws, and the development of algorithms to tackle these aspects (Wriggers, 1995). Various concepts have been explored in the past when simulating interaction or contact behaviour, especially for soil, pile, and raft interactions. The earliest interface elements introduced were the Winkler springs, usually in the form of 1D-interface elements such as $p-y, t-z$, and $Q-z$ springs (Reese et al., 1956; McClelland et al., 1958). These elements have found application in interface modelling for piled rafts, as utilized by Griffith et al. (1991), Poulos (1994), Russo (1998), Kim et al. (2001) and several others.

Goodman et al. (1968) introduced the concept of zero thickness interface elements, but their implementation necessitated excessively high stiffness values, leading to physical inaccuracies (Desai et al., 1984). Ghaboussi et al. (1973) and Herrmann (1978) made adjustments to enhance the performance of these elements. Bfer (1985) and Gens et al. (1989) subsequently created two- and three-dimensional iso-parametric zero-thickness elements with enhanced numerical capabilities. Zienkiewicz et al. (1970) suggested an alternate approach of using a thin layer interface element, which was further developed by several researchers (Desai et al., 1984; Sharma and Desai, 1992). These elements incorporate a tangent matrix to capture normal, shear, and coupled responses at the interface. Nonetheless, they may not adequately handle significant slip or deformation. Taciroglu et al. (2006) proposed a novel approach by combining one-dimensional frictional, drag, and gap elements in parallel with a nonlinear spring element to represent gap, stick, and slip behaviour at the interface of soil and pile.

Another widely embraced approach is the master-slave concept by Wriggers (1995), which formulates contact geometries and interface constitutive laws for both normal and tangential stress components. This concept is favoured for its realistic response and capability to simulate large deformations. The master-slave concept offers the flexibility to choose between 'node to surface contact' and 'surface to surface contact'. Surface-to-surface contact is generally favoured over node-to-surface contact, supported by evidence from Hibbit and Karlsson (2007). Therefore, this

study uses the master-slave concept, treating the pile and raft as master surfaces and the soil surface as a slave. Furthermore, opting for a penalty-type frictional constraint enforcement method is justified in place of the Lagrange method to define mechanical tangential behaviour, as the latter would increase computational expenses and potentially impede convergence (Hibbit and Karlsson, 2007).

### 3.3.4 Selection of 3D element type

The ABAQUS software offers various element types, including beams, shells, and solids, which can be selected based on the project requirements. Beam elements represent linear structural members like piles or beams within the raft, while shell elements accurately model thin-walled structures such as the raft, although at higher computational cost. Solid elements are essential for representing complex three-dimensional behaviour, particularly for soil, concrete, and stress concentrations in structural interactions. Figure 3.4 illustrates the solid element options available for three-dimensional analyses. Among these options, the hexahedral element offers greater accuracy and involves less computation compared to the four-noded tetrahedral and six-noded triangular wedge element, having a continuum of the same volume. Hexahedral elements may either have 8 or 20 nodes, depending upon the nature of the project. The manual (Abaqus/CAE User's Manual) suggests using 20-noded elements for bending-dominated models, whereas 8-noded elements are advised for models with complex interactions.

The hexahedral element is a suitable choice for the consistent shape of the soil continuum and raft. Tetrahedral and wedge-shaped elements provide better discretization when dealing with the widely used circular piles. The observation that simulating square piles saves significant time suggests that converting other cross-sections, such as circular or octagonal ones, into equivalent square piles is a viable option. However, if time is not a critical constraint, it is always preferable to model the pile with its actual cross-section. The present study utilized the eight-node hexahedral element due to its simplicity, larger adaptability and lesser computational

time.

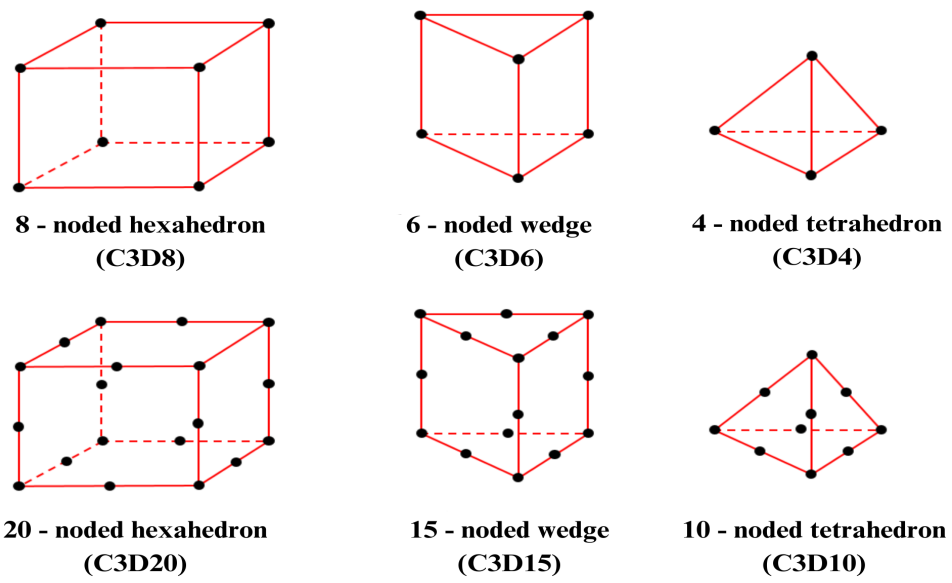


Figure 3.4: Visual representation depicting solid elements

### 3.3.5 Meshing of the model

Meshing involves interconnecting elements through shared nodes in a finite element model. The relationship between result accuracy and computational requirements is delicate; a denser mesh improves accuracy but also adds to computational complexity. Hence, the determination of mesh density is vital, as it harmonizes computational resources and precision. For complex piled raft and soil shapes, it is recommended to partition them into simpler subdomains due to ABAQUS's limitations. Given ABAQUS's absence of automated mesh generation for complex geometries, an alternative method was adopted. The subdomains are divided and refined manually or semi-automatically, focusing on critical zones. After assigning boundary conditions and material properties, the quality of the mesh is verified before initiating the simulation.

In ABAQUS software, a variety of mesh types are available to discretize geometries for numerical analysis. These include structured and unstructured meshes, tetrahedral and hexahedral meshes for 3D models, and quadrilateral/triangular

meshes for 2D simulations. Additionally, mixed meshes combine different element types for efficiency. Adaptive meshes adjust density during simulation, while layered meshes suit composite materials. For symmetric structures, sweep meshes are useful. The choice of mesh type balances accuracy and computation, often requiring experimentation to find the optimal configuration.

### 3.3.6 Step time incrementation

Analyses are organised in ABAQUS to adhere to a particular load application sequence, defined through various steps. The geostatic step, which succeeds the initial step, establishes equilibrium with gravitational stresses. The subsequent steps accommodate the application of external loads. The step time increment, which is the same for strain-controlled and stress-controlled analysis, typically determines the load application in a step.

During the analysis process, field variables like reaction forces, stresses, and displacements are meticulously tracked with each incremental step. Yet, situations arise where a step encounters notable deformation, potentially causing ABAQUS to falter in its convergence and thereby terminating the analysis prematurely. This challenge becomes especially pronounced during considerable deformations, as the step increment in ABAQUS converges towards the defined minimum value in the step formulation, leading to resource-intensive simulations.

Therefore, conducting an initial investigation becomes a valuable practice to assess the impact of step time increments on analysis results, ultimately aiding in the reduction of computational expenses.

## 3.4 Validation of the model

Validating the model is a crucial step in the finite element analysis (FEA) process, ensuring that the numerical simulation accurately reflects the actual behaviour of the physical system. The validation process aims to guarantee the accuracy and

reliability of the developed model, and it often draws upon information from the literature and laboratory tests for the properties used in the numerical validation.

The present section aims to develop a three-dimensional model of a piled raft foundation embedded in soil. The model's geometry and material properties were sourced from the work by Vakili (2015) to achieve this. The relevant parameters are summarized in Table 3.1 and Table 3.2 for reference. Table 3.1 provides an overview of the model's geometry, while Table 3.2 outlines the associated material properties. The results obtained from a specific case of the experimental study were compared to validate the developed model.

Table 3.1: Geometry of the model (Vakili, 2015)

| **Pile configuration** | **Size of soil continuum** $(mm)$ | **Raft dimensions** $(mm)$ | **Square pile dimensions** $(mm)$ |
|---|---|---|---|
| $PR\_1 \times 1$ | $500 \times 500 \times 600$ | $100 \times 100 \times 25.4$ | $22.4 \times 22.4, 290(d_p)$ |

Table 3.2: Material properties for the model (Vakili, 2015)

| **Properties** | **Soil** | **Raft** | **Pile** |
|---|---|---|---|
| **Elastic modulus** $(N/m^2)$ | $1.3 \times 10^7$ | $2 \times 10^{11}$ | $2 \times 10^{11}$ |
| **Poisson's ratio** | 0.25 | 0.3 | 0.3 |
| **Density** $(kg/m^3)$ | 1554 | 7800 | 7800 |
| **Load** | Self-weight | Self-weight | Self-weight $+41.8N/cm^2$ |

Equivalent cross-sectional areas exhibit minimal variation in numerical response variation, rendering the adoption of a simpler geometry for modelling an effortless and efficient procedure (Sinha, 2013). Hence, the simulation prioritised simplicity by employing square piles instead of circular piles for modelling.

Figure 3.5 depicts the numerical model of the soil and piled raft foundation, featuring pile configuration of $1 \times 1$. These models were then assigned the respective material properties and assembled with the supporting soil.

While defining the soil properties, Young's modulus of elasticity for the soil ($E_{sand(kPa)}$) was determined using the following expression (Bowles, 1987):

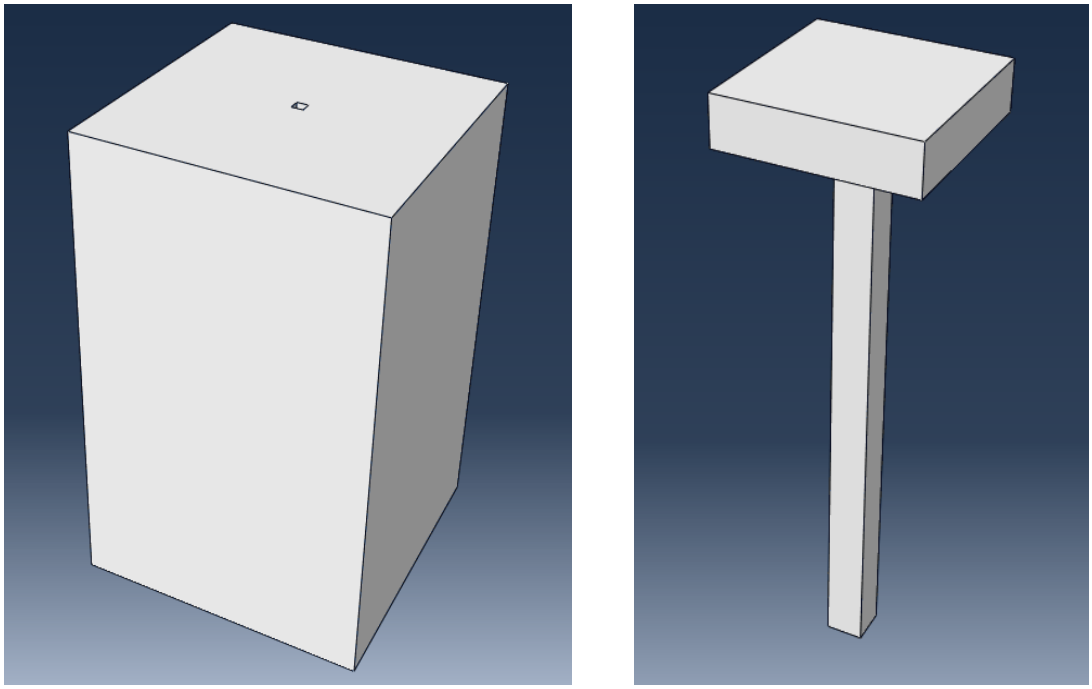

(a) Soil model (b) Piled-raft model ($1 \times 1$)

Figure 3.5: Part modelling in ABAQUS

$$E_{sand(kPa)} = 500(N_{60} + 15) \tag{3.7}$$

$N_{60}$ denotes the adjusted blow count observed using the Standard Penetration Test. Based on existing literature, the elastic modulus and Poisson's ratio fell within the range of $10 - 50MPa$ and $0.25 - 0.40$, respectively. Therefore, adopting the corresponding values of $13MPa$ and 0.25 for the study can be considered reasonable.

Figures 3.6a and 3.6b illustrate the mesh in its undeformed and deformed states for the first model, i.e. $PR\_1 \times 1$. Furthermore, figures 3.7 and 3.8 represent the displacement in both sectional and three-dimensional views for the particular case.

Figure 3.9 displays the outcomes of the conducted numerical analysis. The figure showcases a comparison between the experimental and numerical results from the existing literature and the developed model utilizing both linear-elastic and non-linear plastic models. Notably, the figure reveals a high level of agreement, indicating a strong consistency achieved through the developed numerical model. However, it also shows that the pattern of non-linear analyses resembles more to the

experimental results.

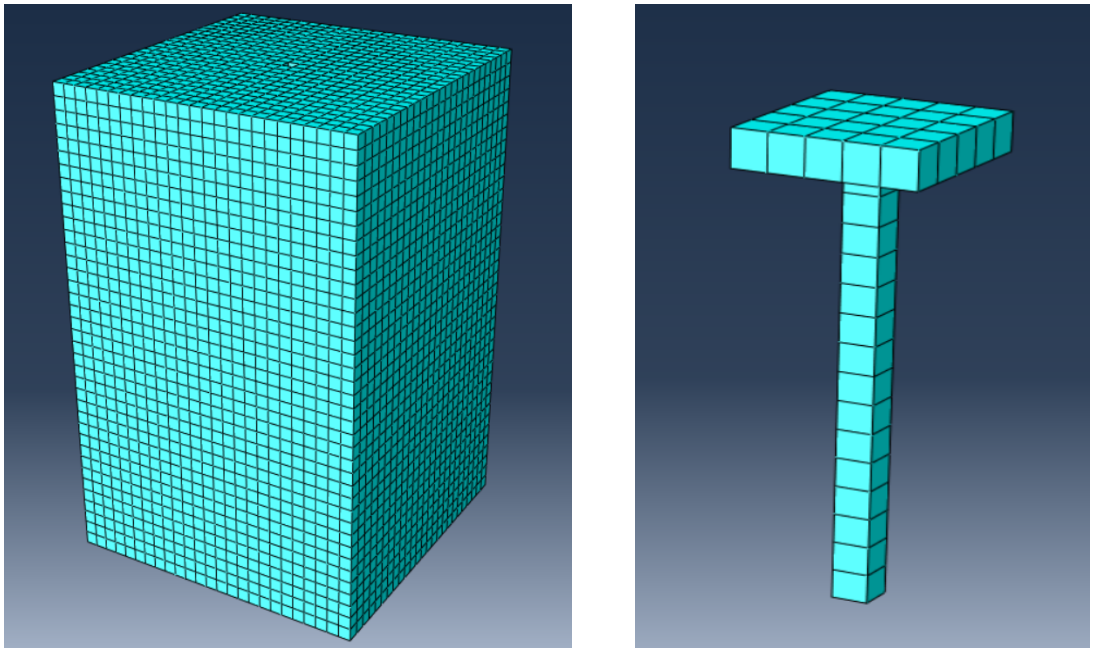

(a) Soil model (b) Piled-raft model ($1 \times 1$)

Figure 3.6: Meshing of the models in ABAQUS

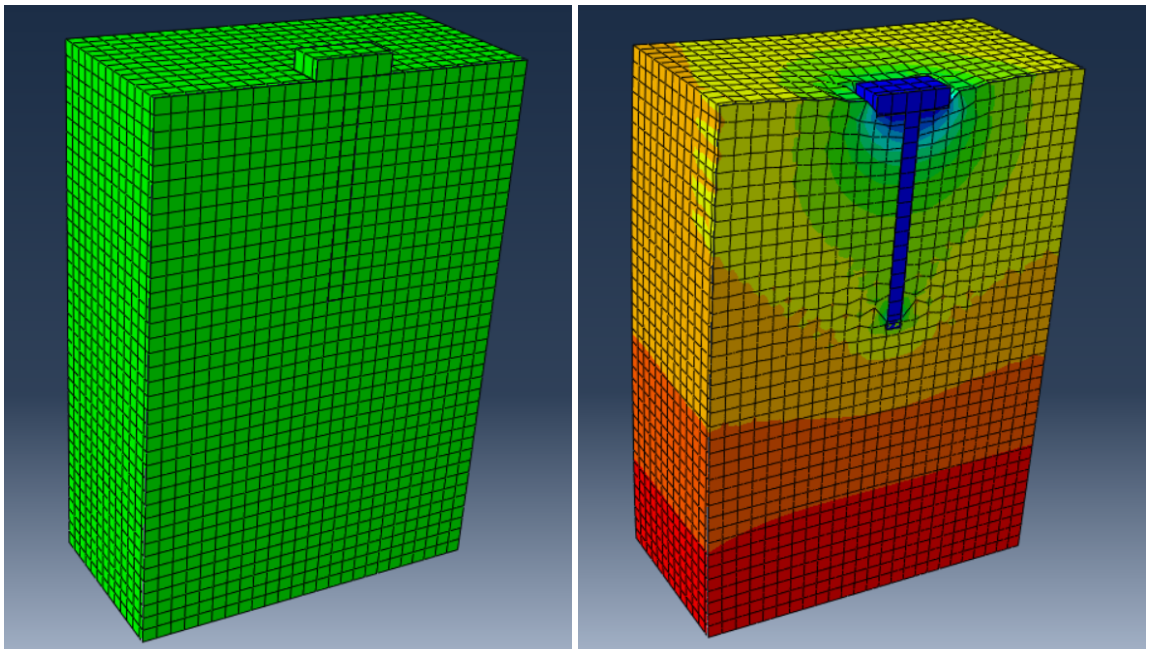

(a) Soil model (b) Piled-raft model ($1 \times 1$)

Figure 3.7: Three-dimensional cut view of displacement contours (Validated model)

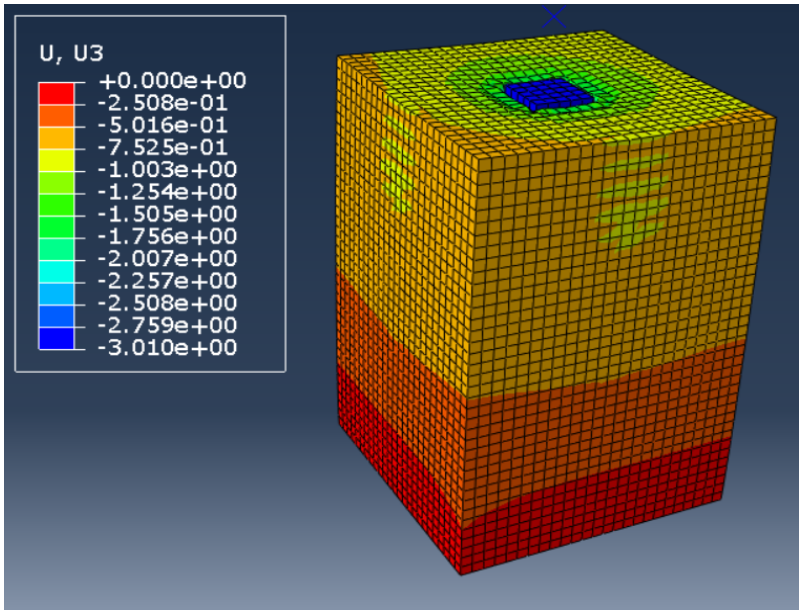


Figure 3.8: Three-dimensional view of displacement contours (Validated model)

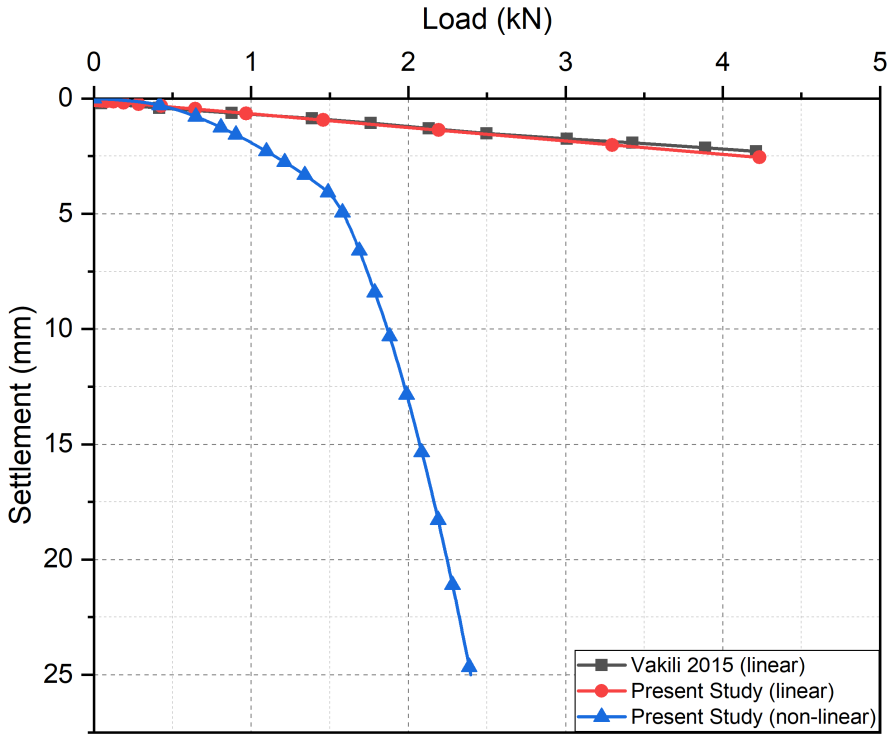


Figure 3.9: Model Validation

## 3.5 Parametric analysis of piled raft foundation

Piled raft foundations involve complex interactions among design parameters like pile arrangement, raft dimensions, soil characteristics, and load conditions. Parametric analysis offers a systematic method to explore various parameter

combinations, optimizing foundation performance while ensuring safety and stability. Customization is key in addressing diverse project needs and complexities. Parametric analysis empowers engineers to tailor foundation designs to site-specific conditions, structural loads, and soil properties. This approach yields highly efficient, cost-effective, and project-tailored foundation solutions.

By altering a single parameter while keeping others constant, researchers can assess the sensitivity of the foundation's behaviour to specific design variables. This procedure facilitates the identification of trade-offs—instances where improving one design aspect could potentially compromise another. For instance, increasing the raft thickness to enhance load distribution might lead to excessive material usage. Parametric analysis assists in harmonizing conflicting design goals by finding a middle way.

It also enables designers to validate their assumptions and predictions through numerical simulations and modeling. Comparing simulation results with analytical expectations, empirical data, or real-world observations enhances confidence in design reliability. Systematic investigation of piled raft foundation behavior across various parameters enhances understanding of underlying mechanisms, load-sharing patterns, and response characteristics, contributing to the field's knowledge.

Table 3.3 presents a diverse range of parameters examined in the current study. These parameters include both geometric properties, such as pile length, pile diameter, number of piles, and raft thickness, as well as soil characteristics, including elastic modulus, friction angle, and Poisson's ratio. The table displays nominal values that serve as references and remain unchanged as any single parameter undergoes variation. Throughout the parametric analysis, the dimensions of the soil continuum were maintained at $25m$ in length, $25m$ in width, and $30m$ in height. Simultaneously, the dimensions of the raft remained fixed at $5m$ in length and $5m$ in width, while its thickness was systematically varied.

In this parametric analysis of piled raft foundations, one-quarter model is adopted to

Table 3.3: Variation of parameters used in parametric study

| **Parameters** | **Variations** | **Nominal value** |
|---|---|---|
| Pile length ($m$) | 10,12,15,18,20 | 15 |
| Pile diameter ($m$) | 0.25, 0.50, 0.75, 1 | 0.50 |
| Number of piles | 0,4,12,16 | 16 |
| Raft thickness ($m$) | 0.25,0.50,0.75,1.00,1.25,1.50 | 0.5 |
| Elastic modulus of soil ($N/mm^2$) | 15,20,25,30,35,40,45,50 | 25 |
| Angle of internal friction ($^\circ$) | 25,30,35,40 | 30 |
| Poisson's ratio of soil | 0.2, 0.25, 0.3, 0.35, 0.4 | 0.30 |

study the behaviour. Circular piles were adopted in the piled raft model. The study addresses soil non-linearity using the Mohr-Coulomb model. This model effectively captures non-linear soil characteristics, facilitating a comprehensive grasp of how the foundation interacts with varying soil conditions. By employing the Mohr-Coulomb model, the analysis strives to accurately represent the complexities of soil behavior and the foundation's performance across diverse scenarios.The remaining procedures align with the previously discussed section. The adopted properties for the simulation are a mass density of 7.39 t/mm$^3$ for the raft and pile, 11.64 t/mm$^3$ for the soil, and a Poisson's ratio of 0.28 for both the raft and pile materials. Boundary conditions were carefully assigned to ensure precise simulation within the ABAQUS framework. Along the line of symmetry, the face conditions were specified to maintain stability: $YSYMM(U2 = UR1 = UR3 = 0)$ and $XSYMM(U1 = UR2 = UR3 = 0)$, signifying symmetry about the corresponding face. Beyond the structure's periphery, the outer soil face was assigned Displacement/Rotation type boundary conditions, effectively restricting movement in lateral directions. Finally, at the model's base, fixed boundary conditions were imposed to signify complete immobilization, indicative of no movement or deformation. A gravity and pressure loading step was created to consider self-weight of the system and any external pressure exerted upon it. The separate representations of the piled raft and the soil continuum can be observed in Figure 3.10, while Figure 3.11 illustrate their assembly.

Meshing used for these models in the present study are presented in 3.12.

The meshing was done properly creating partitioning wherever necessary. A meshing strategy (by size) was employed in the lateral direction with element sizes ranging from 15(minimum) to 30(maximum) in lateral direction, with a finer mesh surrounding the piled raft and a coarser mesh in areas farther from it. In the vertical direction, the element size was set at 15 unit. Circular piles were simulated using hexahedral elements and the medial axis algorithm for accurate representation of their geometry. The simulation employed a local seed by number approach, considering circular piles with a total of 8 elements positioned around the circle. A reference settlement of 40mm was fixed using tie constraints to assess bearing capacity under varying geometric and soil conditions.

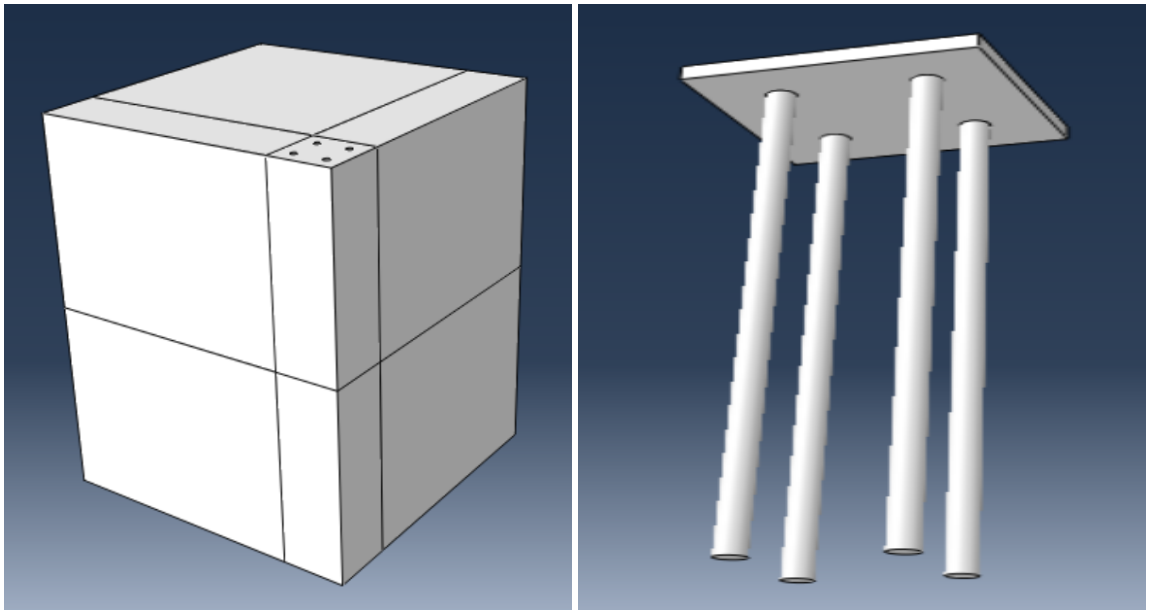

(a) Soil continuum (b) Piled raft

Figure 3.10: Modelled part for the present study

Finally, the influence of these parameters on the performance of the piled raft was evaluated by analyzing load-settlement curves. Load-settlement curves are used in piled raft foundation analysis to assess foundation performance under varying loads, determine bearing capacity, and optimize design by studying settlement behavior and comparing different foundation configurations. In this context, 'settlement' refers to the vertical displacement of the raft relative to the underlying supporting soil.

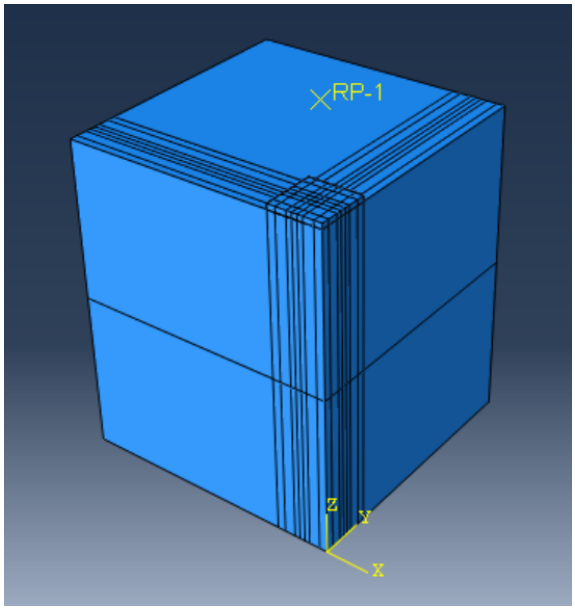


Figure 3.11: Assembly of the modelled parts

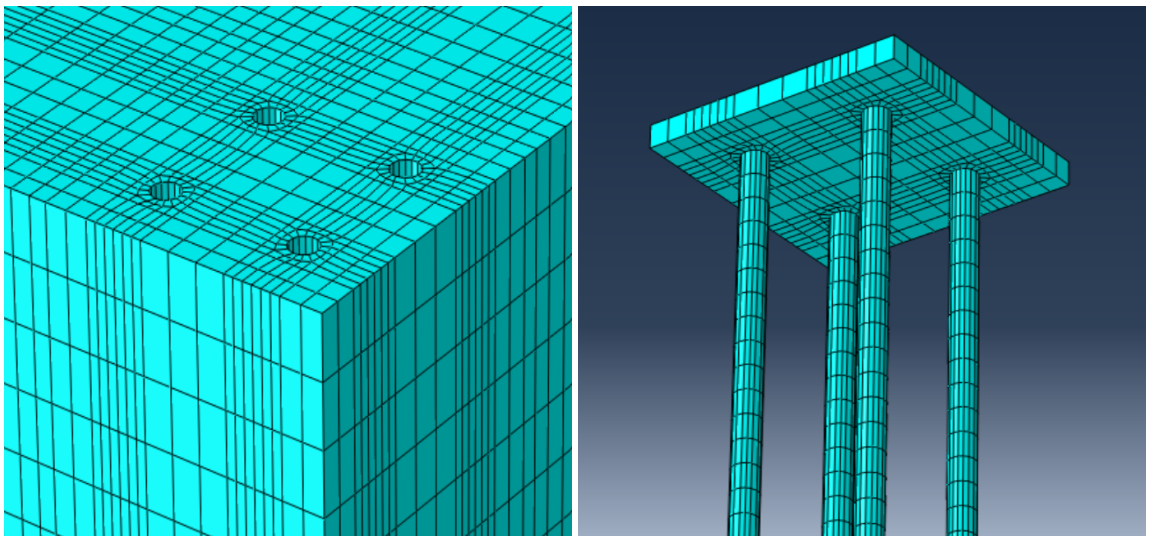

(a) Soil continuum (b) Piled raft

Figure 3.12: Meshing used in the present study

### 3.5.1 Effect of length of piles ($L_p$)

Longer piles generally contribute to increased load-carrying capacity. As the pile length increases, the additional embedded length provides greater resistance against vertical loads, consequently indicating higher stiffness and enhanced load-bearing capability. Pile length also plays a role in controlling settlement. Longer piles can limit the magnitude of settlement by offering increased support to the foundation. This effect is evident in the gradual progression of the load-displacement curve,

demonstrating reduced settlement as pile length increases.

Figure 3.13 illustrates the fluctuation in pile length across values of $10m, 12m, 15m, 18m$, and $20m$. It is evident that as the pile length extends from $10m$ to $20m$, there is a noticeable enhancement in load-bearing capacity, amounting to an approximate 60% increase.

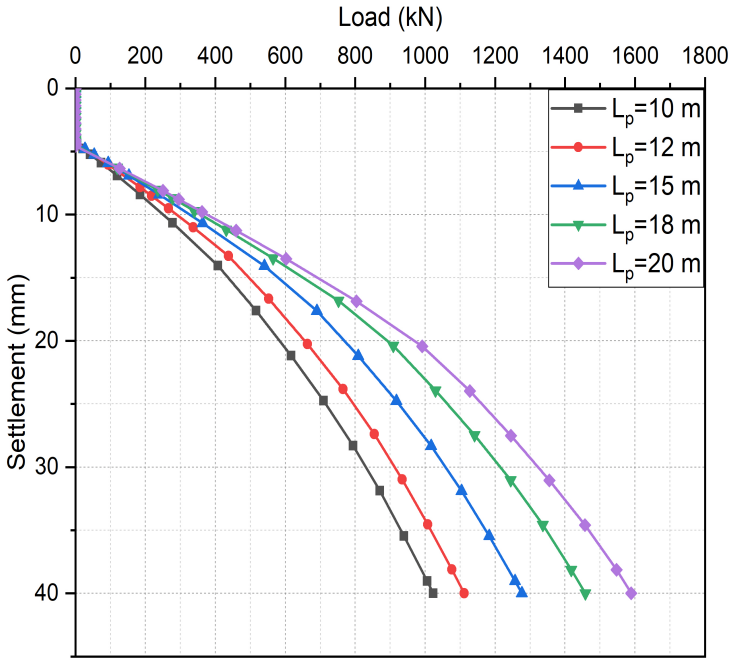


Figure 3.13: Effect of length of piles ($L_p$) in piled raft

### 3.5.2 Effect of diameter of piles ($d_p$)

Larger diameter piles offer increased surface area in contact with the soil, leading to greater mobilization of soil resistance. This, in turn, results in enhanced load-carrying capacity. As pile diameter increases, the foundation can support higher vertical loads.

Similar conclusions are drawn from the study (Figure 3.14), which illustrates variations in pile diameters, including $0.25m, 0.50m, 0.75m$, and $1m$. It is evident that considering a diameter of $0.25m$ as a reference, there is an observable percentage increase in load-bearing capacity with each subsequent $0.25m$ increment. These increments result in approximate increases of $83\%, 200\%$, and $315\%$, respectively.

Nevertheless, as the diameter increases by $0.25m$ in each step, the subsequent rise in the percentage increase diminishes, initially 83%, followed by 64%, and ultimately 38%. This suggests that an increase in diameter remains reasonable up to a certain point, beyond which further increments in diameter would yield negligible gains.

Although larger diameter piles provide advantages in relation to load-carrying capacity and stiffness, they might pose construction difficulties. These larger piles necessitate greater excavation and handling efforts, potentially resulting in extended construction duration and escalated costs.

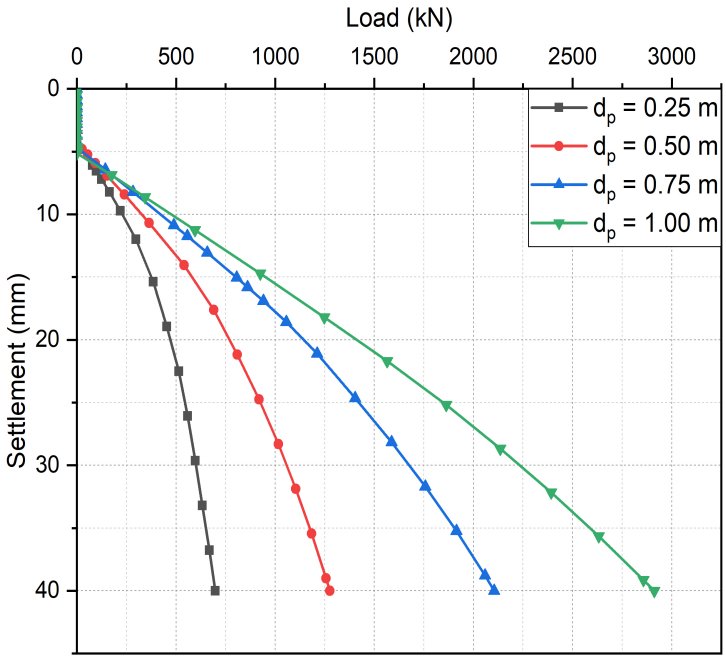


Figure 3.14: Effect of diameter of piles ($d_p$) in piled raft

### 3.5.3 Effect of friction angle ($\phi$)

The angle of internal friction significantly influences two key aspects of piles: skin friction along the shaft and end-bearing capacity at the base. Higher friction angles enhance both skin friction and end-bearing capacity, boosting the load-carrying potential of piled raft foundations. Load-settlement curves with higher friction angles demonstrate greater load-bearing capacities and possibly reduced settlements under similar loads due to increased stiffness. Higher friction angles correspond

to increased ultimate bearing capacities, affecting the shape and slope of load-settlement curves.

In this study, the angle of internal friction was varied systematically: 25°, 30°, 35°and 40°(Figure 3.15). An incremental increase from 25°to 40°led to noticeable improvements in load-bearing capacity. Specifically, capacity increased by 10% from 25°to 30°, and significantly by 16.5% and 21.5% at 35°and 40°, respectively. Notably, the rate of improvement declined as friction angles increased, with subsequent increments showing enhancements of 10%, 5.5%, and 4.4%. This trend aligns with findings in existing literature (Sinha, 2013).

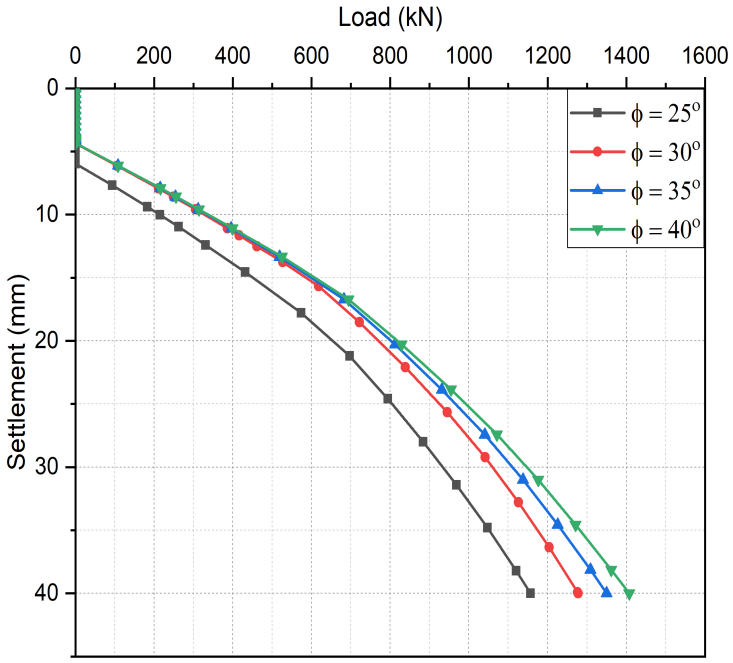


Figure 3.15: Effect of friction angle of soil ($\phi$) in piled raft

### 3.5.4 Effect of elastic modulus of soil ($E$)

A higher elastic modulus signifies stiffer soil, leading to more balanced load distribution between the raft and piles. This distribution is critical in determining the contribution of each component to supporting the structure. Additionally, the soil's elastic modulus affects the extent of settlement experienced by the foundation -stiffer soil tends to exhibit reduced settlement due to its enhanced resistance to deformation.

Figure 3.16 depicts the variation in soil's elasticity modulus, spanning from $15MPa$ to $50MPa$. As the modulus progresses in $5MPa$ increments, a concurrent improvement in load capacity is evident. Notably, the load capacity experiences significant percentage enhancements at each step: 16%, 10.35%, 7%, 6.6%, 5.5%, 4.5%, and 4.3%. It is worth noting that this upward trend tends to stabilize as the soil attains a specific level of stiffness.

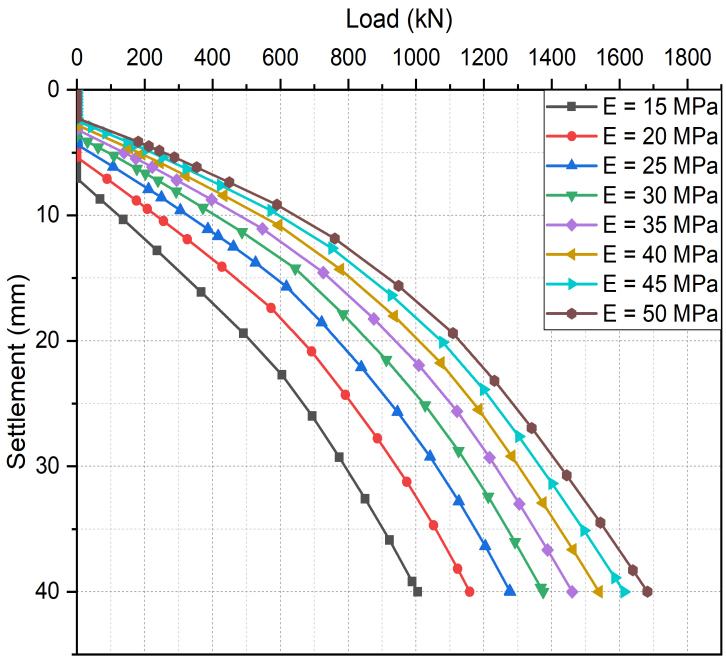


Figure 3.16: Effect of elastic modulus of soil ($E$) in piled raft

### 3.5.5 Effect of Poisson's ratio ($\nu$)

Poisson's ratio, representing the ratio of lateral strain to axial strain, directly affects the deformation behaviour of soil and the foundation's response to applied loads. As Poisson's ratio increases, the lateral expansion of the soil under load becomes more pronounced, impacting the distribution of stresses within the foundation system. Consequently, altering Poisson's ratio leads to distinctive load-settlement curves, showcasing varying degrees of settlement under the same load increments.

In this ongoing study, Poisson's ratio is routinely varied across a spectrum spanning from 0.25 to 0.40, covering specific values of 0.25, 0.30, 0.35, and 0.40 (Figure 3.17). The results reveal that load capacity likewise exhibits an increase as Poisson's

ratio rises. However, within this range, the observed percentage rise in load capacity fluctuates modestly, ranging between approximately 1.5% and 2.5%. This suggests that Poisson's ratio exerts a comparatively milder influence compared to other influential parameters in the context of load-settlement curves for piled raft foundations.

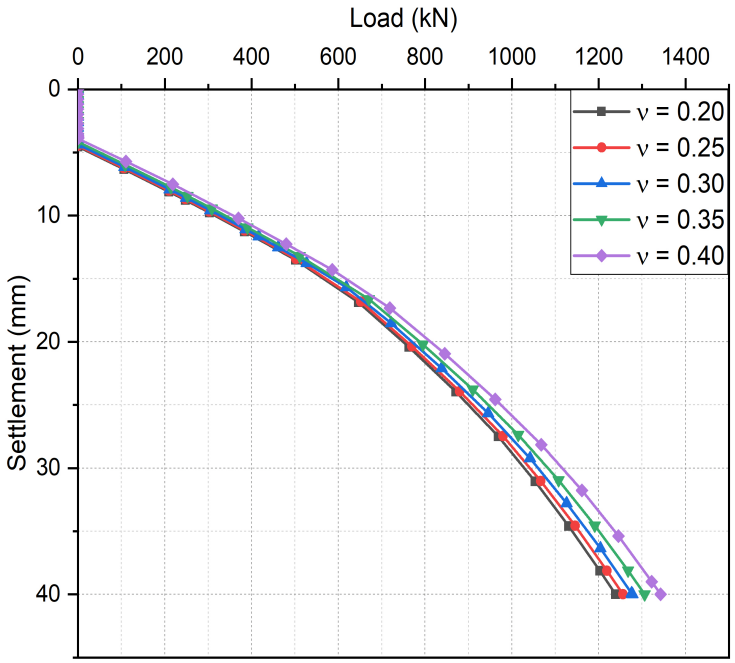


Figure 3.17: Effect of Poisson's ratio of soil ($\nu$) in piled raft

### 3.5.6 Effect of number of piles ($n_p$)

The number of piles in a piled raft foundation directly impacts its load-carrying capacity and settlement behaviour. Increasing the number of piles generally enhances the foundation's overall capacity due to increased load distribution and reduced pile loads. With an increase in the number of piles, load distribution becomes more uniform across the foundation, reducing individual pile loads. This improved load-sharing capability directly contributes to higher load-carrying capacities.

This effect is evident in load-settlement curves (Figure 3.18) of piled rafts with 4, 12 and 16 piles and unpiled raft. Here piled rafts with more piles tend to show higher initial stiffness and greater load-bearing capacities.

In contrast to an unpiled raft, which can support a load of $7.5kN$ with a settlement of $40mm$, piled rafts with 4, 12, and 16 piles exhibit load-bearing capacities of approximately $8kN, 9.5kN$ and $12.8kN$, respectively.

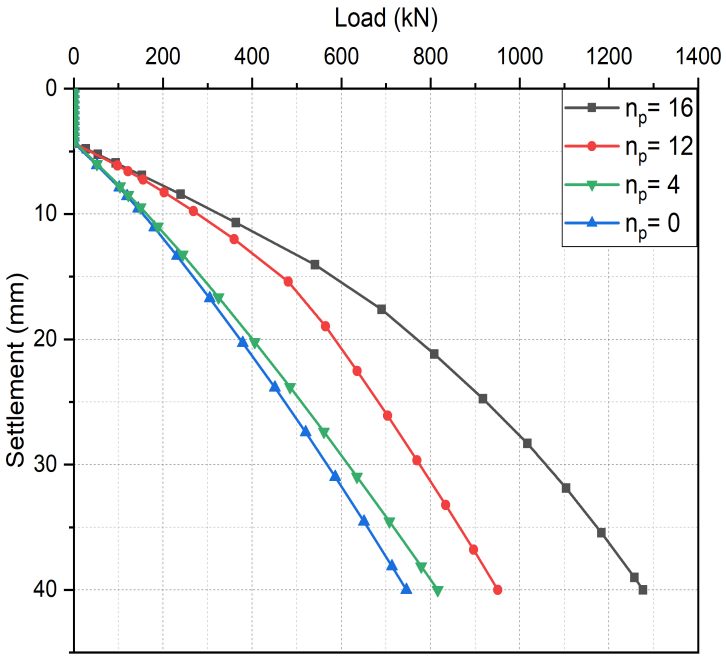


Figure 3.18: Effect of number of piles ($n_p$) in piled raft

### 3.5.7 Effect of raft thickness ($t_r$)

The variation in raft thickness holds substantial influence over the load-settlement characteristics of piled raft foundations. Thicker rafts inherently bestow greater load-carrying capacity, diminished settlements, and stiffer response.

Illustrated through the array of load-settlement curves corresponding to various raft thicknesses, ranging from 0.25m to 1.50m (depicted in Figure 3.19), this parameter significantly shapes the performance of the foundation. A noticeable trend becomes evident: with an increase in raft thickness, measuring $0.25m, 0.50m, 0.75m, 1m, 1.25m$ and $1.5m$, there is a corresponding rise in load-bearing capacity. Yet, it is notable that thicker rafts exhibit a comparatively higher initial settlement, a phenomenon attributed to the self-weight of the raft (Sinha, 2013).

Thus, the magnitude of raft thickness becomes a pivotal consideration in optimizing the structural design and performance of piled raft foundations across diverse geotechnical scenarios.

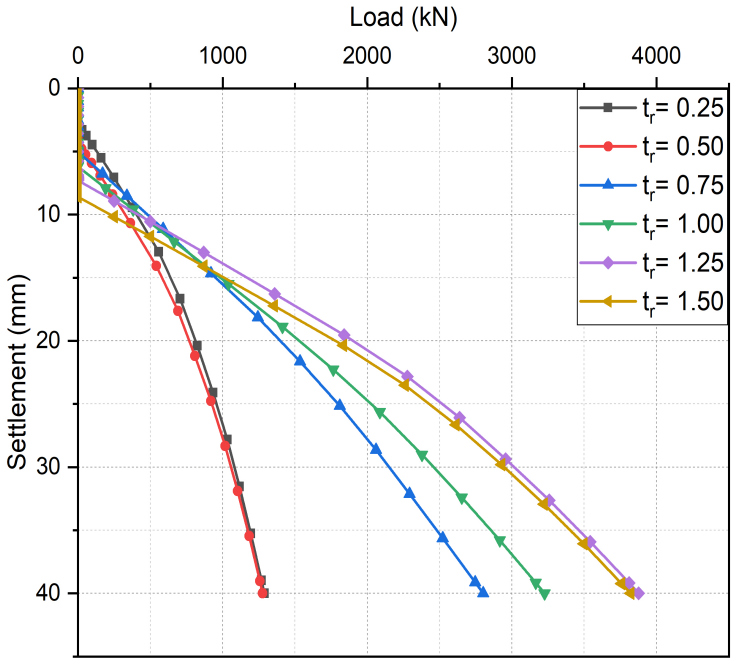


Figure 3.19: Effect of raft thickness ($t_r$) in piled raft

## 3.6 Summary

An investigation using a $3D$ finite element approach was carried out to comprehend the performance of substantial piled raft foundations on sandy soil. Derived from the outcomes of the finite element analysis, the subsequent deductions can be made:

- Increased pile length enhances both load-bearing capacity and stiffness while reducing the settlement. It is worth noting that there is a significant increase of almost 60% in the load-bearing capacity when the length of the pile increases from $10m$ to $20m$.
- Load-settlement curves revealed a significant correlation, indicating that higher values of Poisson's ratio were associated with increased load-bearing capacities. Notably, this augmentation ranged from 1.5% to 2.5% within the specified range of Poisson's ratio, which was between 0.2 and 0.4.

- Elevated friction angles enhance skin friction and end-bearing capacity, leading to elevated load-bearing capacity and reduced settlements in load-settlement curves. The angle shift from 25°to 30°resulted in a 10% load capacity increase, followed by substantial rises of 16.5% at 35°and 21.5% at 40°. This pattern demonstrates diminishing percentage enhancements as friction angles increase, with subsequent adjustments yielding improvements of 10%, 5.5%, and 4.4% respectively.

- In comparison to a reference diameter of $0.25m$, the load-bearing capacity exhibits constant and significant percentage improvements with each successive $0.25m$ increment. These increments lead to approximate enhancements of 83%, 200%, and 315% correspondingly. Nevertheless, as the diameter increases by $0.25m$ in each successive stage, the succeeding percentage growth gradually decreases: commencing at 83%, followed by 64%, and ultimately reaching 38%.

- An increase in elastic modulus from $15MPa$ to $50MPa$ results in a stiffer soil, enabling it to resist applied loads more effectively. This leads to a typical increase in the foundation's load capacity, with observed percentage increases ranging from 16% to 4.3% for every $5MPa$ increase.

- The number of piles in a piled raft foundation significantly influences its load-carrying capacity and settlement behavior. Increasing the number of piles results in improved load distribution leading to higher load-bearing capacities. This is evident in load-settlement curves, where piled rafts with more piles exhibit greater initial stiffness and increased load-bearing capacities compared to unpiled rafts. For instance, with respect to an unpiled raft with a settlement of 40mm, the bearing capacity of piled rafts with 4, 12, and 16 piles increases by approximately 6.6%, 26.67%, and 70.67%, respectively.

- The impact of raft thickness on piled raft foundations is significant. Thicker rafts enhance load-carrying capacity and stiffness while reducing settlements,

although they may initially experience higher settlements due to self-weight. The current research showed a 200% load capacity increase as raft thickness progressed from $0.25m$ to $1.5m$. Nonetheless, it is crucial to carefully optimise the thickness increment to ensure cost-effectiveness.

It is crucial to acknowledge that the benefits of increasing most parameters tend to diminish once specific thresholds are reached. This underscores the importance of adopting a careful approach when making adjustments to these parameters in order to achieve optimal load-bearing capacity, while also ensuring efficiency and cost-effectiveness.